Paintable Films from Chemically Exfoliated 2D Bismuth Telluride Nanosheets

Elaine Carroll[1], Darragh Buckley[1], Gillian Collins[1], Justin D. Holmes, Kafil M. Razeeb[2], and Colm O'Dwyer[1,2]*

[1] *Department of Chemistry, University College Cork, Cork, Ireland*
[2] *Tyndall National Institute, Lee Maltings, Cork, Ireland*

This work highlights a method whereby solvent exfoliation of Bi_2Te_3 into solution-dispersible 2D nanosheets can form a practical thin film that can be distributed across a surface. Optimized exfoliated suspensions are also shown to form smooth, uniform blends when mixed with poly ethylene glycol and other polymers to produce a paintable Bi_2Te_3 film that can be applied to surfaces using an innovative painting technique. Atomic force microscopy, transmission electron spectroscopy, Raman scattering spectroscopy and scanning electron spectroscopy are used to examine the structure of the 2D nanosheets and the Bi_2Te_3 thin films. Electrical transport studies show that the films have conductive pathways over a range of surfaces and various structural formations, linking the conductivity to the percolating conduction through the nanosheet ensemble.

Introduction

There is a significant need for site-specific and on demand cooling in electronic, optoelectronic and bioanalytical devices, where cooling is currently achieved by the use of bulky and/or over-designed system-level solutions (1, 2). Thermoelectric devices can address these limitations by nanostructured layered thermoelectric (TE) materials with enhanced figures of merit (ZT). The figure of merit $ZT = S^2\sigma T/K$, where $S=-\Delta V/\Delta T$ is the Seebeck coefficient (ΔV is the voltage difference caused by a temperature difference ΔT), σ is the electrical conductivity and K is the thermal conductivity. Ideally, the figure is maximized by processes that contribute to large electrical conductivities, while reducing or maintaining as low a thermal conductivity as possible. (3-5)

Layered materials represent a diverse source of two-dimensional (2D) systems with exotic electronic properties and high specific surface areas that are important for sensing, catalysis, and energy storage applications(6-8). Bi_2Te_3 is of particular interest as it is both a topological insulator and thermoelectric material. Bulk Bi_2Te_3 is one of the principal industrial thermoelectric materials because Bi_2Te_3-based materials have the highest thermoelectric figure of merit, ZT between 1.1-1.2 at room temperature (9, 10)(11).

In terms of electrical conductivity control, quantum confinement of charge carries in quantum wells can lead to a considerable ZT improvement as the carrier density-of-states (DOS) near the Fermi level is boosted to increase the resultant thermopower (12, 13), but this is dependent

on a material being crystalline, and with thicknesses on the order of few atomic layers. To fulfil these conditions, 2D nanosheets that maintain or enhance their direct-gap semiconductivity with a high carrier density are potentially very useful. Low-dimensional structures in principle, should also contribute the other necessary effect to increase the ZT, i.e. reduce the thermal conductivity through spatial confinement of heat-carrying acoustic phonons. At the same, disorder can negatively affect electron mobility and affect electrical conductivity via electron scattering, thereby preventing maximum ZT enhancement. In order to become more useful these layers need to be exfoliated down to smaller dimensions, such as its 2D form (nanosheets), its thermoelectric response improves when the overall nanostructured composite approximates an electronic crystal, but behaves in tandem as a phonon glass. Slowing the acoustic phonon group velocity through confinement, and introducing grain boundary and point defect contacts to enhance the reduction in thermal conductivity is possible if suitable materials preparation methods for 2D nanosheets can be developed.

Many methods have been used by others to create thin films of bismuth telluride and its related polymorphs, and a wide range of graphene-like materials and methods(14-20). Co-evaporation of bismuth and of telluride(21) ion-beam sputtering deposition(22), electrochemical deposition (23), along with many more. However the method that interested us was chemical exfoliation due to the recent advances in this area for high-through and high quality dispersions of graphene and related 2D TMD's for example. (7, 8, 24, 25)

Here, we demonstrate a method whereby solvent exfoliation of Bi_2Te_3 into solution-dispersible 2D nanosheets can form a practical thin film that can be distributed across a surface. Optimized exfoliated suspensions are also shown to form smooth, uniform blends when mixed with poly ethylene glycol and other polymers to produce a paintable Bi_2Te_3 film that can be applied to surfaces using an innovative painting technique. Atomic force microscopy, transmission electron spectroscopy, Raman spectroscopy and scanning electron spectroscopy show that the structure of the 2D nanosheets dispersed within a polymer are highly reproducible Bi_2Te_3 thin films. Electrical transport studies confirm that the films are conductive. Electron transport pathways over a range of surfaces and various structural formations, link the conductivity to the percolating conduction through the nanosheet ensemble. The combination of the facile preparation method and the scope for diverse surface coating as a cohesive and conductive thin film offers a methods for integration with heat producing devices for energy harvesting applications.

Experimental

Preparation of Bi_2Te_3 nanosheet dispersions

Bismuth (III) telluride (Bi_2Te_3) powder, iso propyl alcohol (IPA), NMP and/or CHP were used. All materials were purchased from Sigma-Aldrich and used as supplied. Bi_2Te_3, NMP/CHP and IPA were added to a round bottomed flask in varying ratios of 1:2:15 (1:1:15/2:1:15), heat was then supplied (423 K) and the mixture was refluxed for 6 h under stirring. It was then allowed to cool for ~1 h, and was and subsequently distilled for 24 h.

Processing of nanosheet paints

Various combinations of sonication, centrifuge (and annealing) and drop casting, spin coating etc. were used to disperse Bi_2Te_3 nanosheets. 1-cyclohexenyl pyrrolidine (CHP) and N-methyl-2-pyrrolidone (NMP) were used as solvents. After the preparatory distillation step, polyethylene

glycol (PEG, M_w = 400 g/mol) was added to each mixture and subsequently allowed to cool while being stirred continuously for 60 minutes. The mixtures were then sonicated for 90 minutes. The mix was then centrifuged at 4500 rpm for 45 min. For each nanosheet dispersion, the supernatant was removed and the mixture was then painted onto substrates (glass, Si and SiO_2) of known areas. The material was distributed evenly across the glass slides in predetermined aspect ratios that allow examination of length/width dependence. The substrates were then annealed at 100^{o}C for 3 h. At the conclusion of the preparation cycle a thin film of Bi_2Te_3 that was flaky in appearance was produced.

Materials characterization

Transmission electron microscopy (TEM) was performed using a JEOL 2100 at 200 kV. Nanosheets were dispersed on holey carbon grids. Scanning electron microscopy (SEM) was carried out with a Hitachi S4800 FESEM and FEI Quanta 650 FEG high resolution SEM equipped with an Oxford Instruments X-MAX 20 large area Si diffused EDX detector. Images were collected at operating voltages of 10-20 kV. Raman scattering measurements were acquired using a Renishaw InVia Raman spectrometer using a 514 nm 30 mW Ar^+ laser. Spectra were collected using a RenCam CCD camera. The beam was focused onto the samples using a 50x objective lens. Electrical conductivity measurements were conducted in 2-probe geometry using tungsten probes and In-Ga eutectic metal contacts. I-V curves were acquired at a potential scan rate of 30 mV/s using a BioLogic VSP Potentiostat/galvanostat. Heating was provided directly to the glass substrate for temperature-dependent I-V measurements.

Results and Discussion

SEM images shown in Fig. 1 (a,b) show the thick, bulk flakes that results from mechanical exfoliation and subsequent drop-casting, and AFM analysis of surface-immobilized crystals confirm a layered structure these Bi_2Te_3 flakes. Drop-casting, dip-coating and spin-casting are never found to provide a uniform dispersion of 2D exfoliated sheets when cast on various surface at high or low solution dispersion concentrations. Mechanical exfoliation techniques similar to those used for graphene and some Bi_2Te_3 nanosheet methods produce in consistent sheet sizes and anisotropies. After chemical exfoliation with all solvents the Bi_2Te_3 flakes still retain their crystallinity. HRTEM examination in Fig. 1(d) shows a lattice resolved image from a range of overlapped nanosheets (Fig. 1(e)) comprising the (111) and (011) planes of Bi_2Te_3 with the rhombohedral R-3m space group with D_{3d}^5 point symmetry. The lattice-resolved image in Fig. 1(e) confirms identical crystal structure in regions where thickness contrast is evident, and Moiré fringing from re-stacked nanosheets can be seen in the thicker regions. Exfoliation of nanosheets allows single sheets with varied thickness. Here, the sheet thickness is several molecular layers (quasi-2D) in regions – all nanosheets exhibit identical crystal structure with no in-plane defects, kinks, or layer-on-layer mismatch or changes in registry where more than one molecular layer is present.

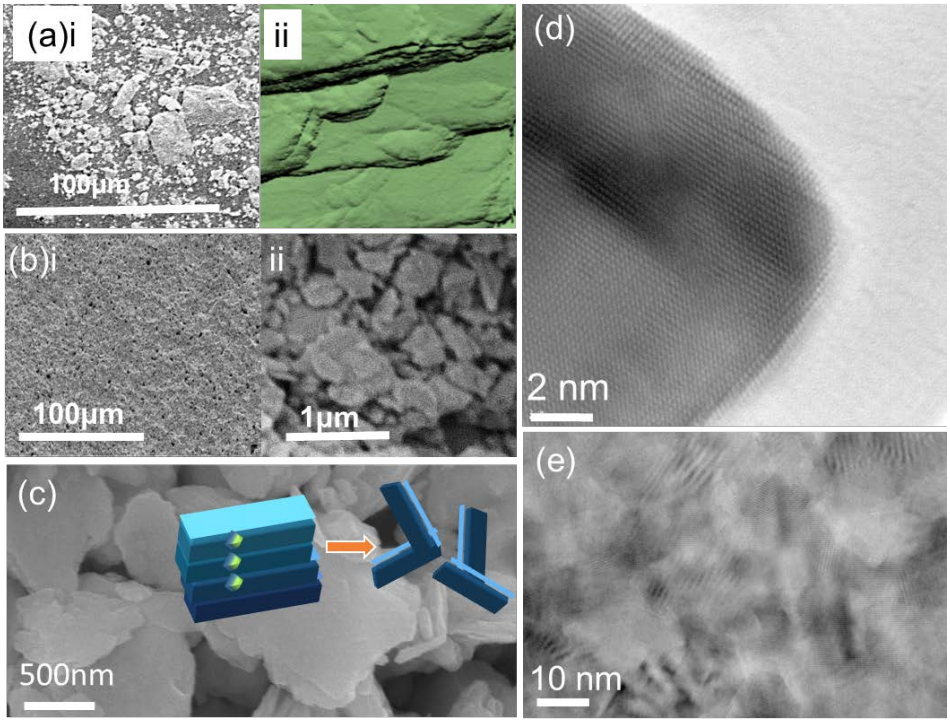

Figure 1 (a) (i) SEM and (ii) AFM images of drop cast Bi_2Te_3 powder. (b) SEM images of a surface deposit of exfoliated Bi_2Te_3. (c) SEM of the layered structure of the Bi_2Te_3 powder. (d,e) HRTEM images

Raman scattering measurements of exfoliated Bi_2Te_3 flakes are presented in Fig. 2. Raman scattering that convolutes the two-fold degenerate E_g and A_{1g} optical phonon modes is sensitive to variations in thickness caused by reduction from 3D to 2D (single molecule thickness). (26-28) The bulk material responds to Raman with two main peaks the E^2_g and the A^2_{1g} these peaks correspond to in plane modes. Exfoliated nanosheets that are a molecular layer thick, i.e. 2D or possibly thinner (3.045 nm corresponding to the $Te^{(1)}$-Bi-$Te^{(2)}$-Bi-$Te^{(1)}$ quintuple), (29) the intensity of Raman tensor for out-of-plane A^1_{1u} and A^2_{1u} modes increases significantly because of symmetry breaking. Exfoliated 2D Bi_2Te_3 is typically described as being either 3D, quasi 2D (several multiple of one molecular layer) or 3D. However, Fig. 2 shows that variations in the intensity of modes can occur due to 2D sheets that are less than 1 quintuple layer thick, or as thick as a fractional multiple of a single layer. Bulk as-received Bi_2Te_3 shows no confinement effect on Raman intensity, and CHP exfoliated sheets are not reduced to 2D thickness even after extended processing [(7, 8)]. NMP-exfoliated nanosheets exhibit characteristic 2D spectra, but the relative intensity of 2D-allowed vibrational modes varies characteristically from sample to sample after optimal chemical and mechanical exfoliation to single or few layer sheets.

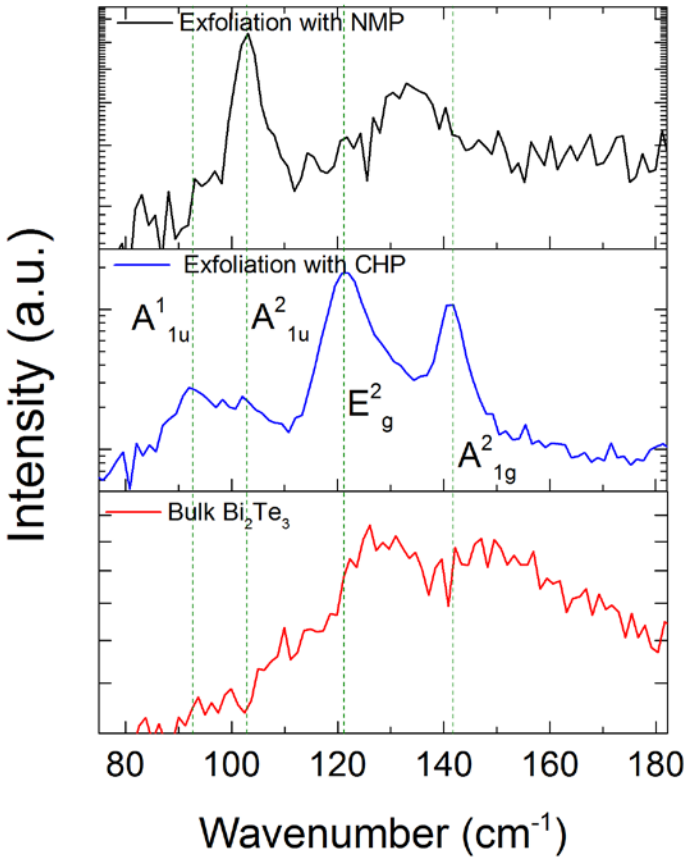

Figure 2 Raman scattering spectra of bulk Bi_2Te_3 powder, CHP-exfoliated and NMP-exfoliated nanosheets.

We then isolated and separate individual nanosheets that show near-perfect crystal quality. The reduced thermal conductivity by crystalline anharmonicity (30) to a lower but finite value (avoiding infinite values associated with divergence in a true 2D material), variations in the thickness of super- and sub-monolayer 2D nanosheets would be advantageous. Ideally, this effect could be facilitated by inhomogeneous exfoliation from bulk where thickness less than and greater than a single molecule are possible within the same nanosheet, possible through bottom up synthetic methods (31). This would provide heat sink regions of quasi-2D Bi_2Te_3 limiting localized hot spots by reduced thermal conductivity caused by altered electron and phonon scattering.

To create electrically conductive materials with reduced thermal conductivity due to confined acoustic phonons with sub- and super-2D thickness variations, phonon scattering and variable thickness stoichiometry variations in nanosheets, a percolating conductive paint method was devised to ensure a ‘bulk’-like quantity of this nanosheet composite using re-stacked sheets in a host polymer (PEG400). The addition of the polymer binds the nanosheets into restacked mismatched superlattice arrangements. (32-37)

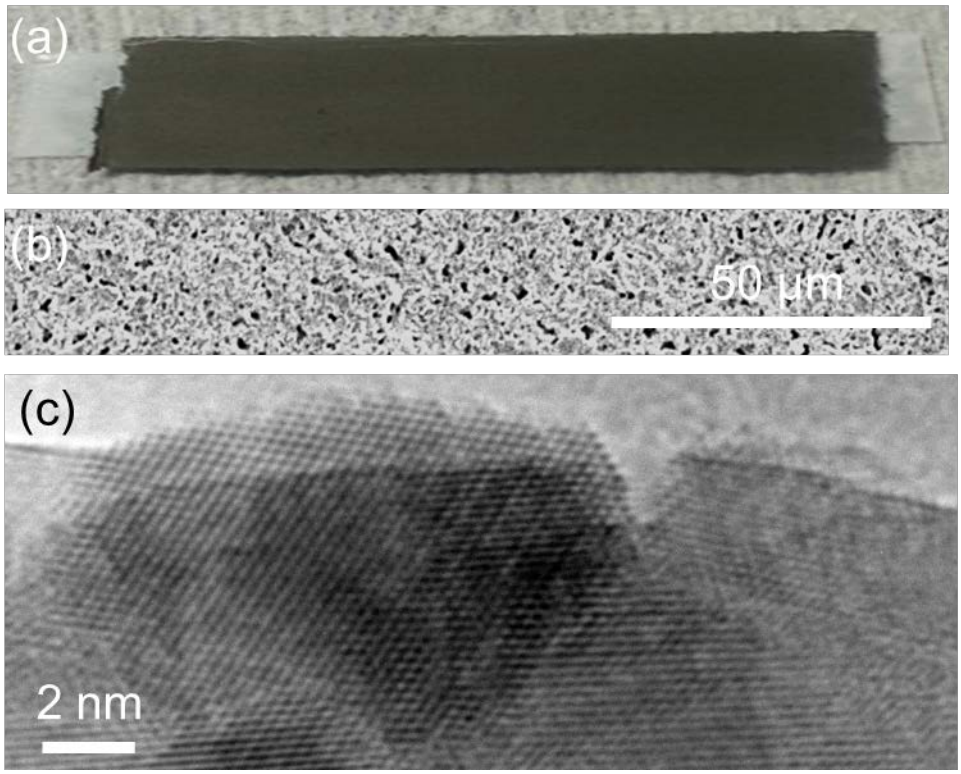

Figure 3 (a) Optical image of the Bi_2Te_3-PEG paint on glass. The strip is ~5 cm long. (b) SEM image of the granular structure of the paint. (c) HRTEM image of the restacked Bi_2Te_3 nanosheets.

The addition of PEG to the nanosheet dispersion created smooth paintable film that uniformly coat various substrates, as shown in Fig. 3(a,b). The internal structure of the paint shows layer upon layer of nanosheets, some microns in length, stacked on top of one another without epitaxial arrangement of layer-by-layer order in the restacking (Fig. 3(c)). The nanosheets are observed to have high energy facets comprising micro-faceted saw-tooth atomic edges. Raman scattering measurement shows that regions of the re-stacked sheets shows 3D characteristics. The sheared and re-stacked nanosheets within the paint retain their nanostructure. Upon mixing with PEG, no intercalation of PEG in a manner similar to organic intercalated within V_2O_5 using primary alkanes or PEG is found. (38-42) Instead, the few-layer nanosheets crystals are encapsulated by a thin layer of PEG as shown in the TEM images in Fig. 4(a). The crystal quality of the few-layer sheets is confirmed through HRTEM analysis shown in Fig. 4(b).

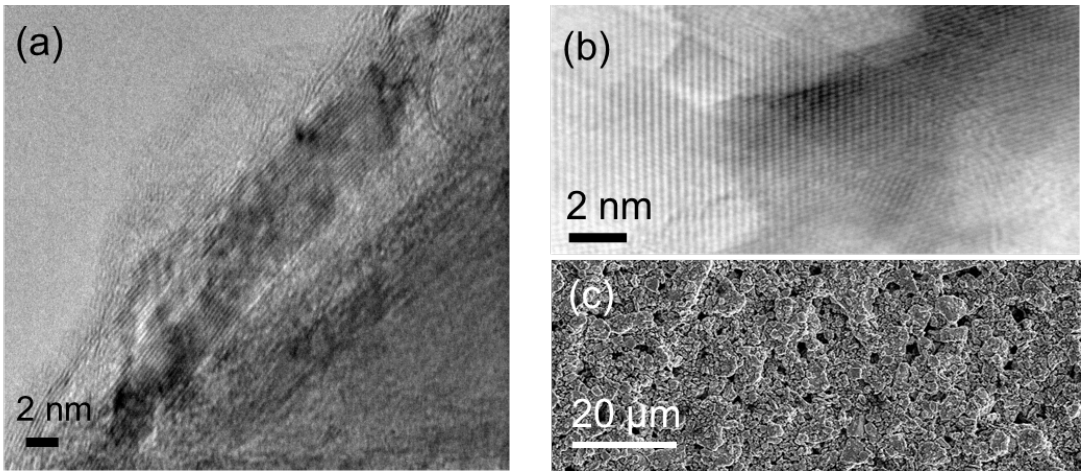

Figure 4 (a) HRETM image of a cross-section of restacked Bi_2Te_3 coated with PEG and (b) plan-view image showing the crystallinity of the stacked nanosheets. (c) SEM image of the surface of the nanosheet paint.

On glass, the electrical characteristics of the nanosheet paint are assessed without leakage currents under the paint. Electrical transport measurements in Fig. 5(a) show that and the painted thin films are ohmically conductive. As PEG itself has very low conductivity of 5.98 pS/cm, and the existence of a current through the composite paint confirms the re-stacked Bi_2Te_3 nanosheets are interconnected and electrical bridge the conduction pathways through the non-conductive host polymer. The conductivity of the nanosheet paint, within a non-conductive host is ~2 µS/cm, but the nominal value is still low due to the density of grain boundaries in a nominally low conductivity material, which does not conduct effectively without either exfoliation that aids in restacking during painting, nor without the non-conducting binder maintaining inter-grain contacts. The higher resistivity value stems a tortuous current path effectively resulting in a percolating conduction path through the nanosheets (43-46). The presence of PEG between the contact ends of encapsulated few-layer nanosheet grains may also contribute to the internal resistance.

Upon reducing nanosheets in dimension to approach quantum wells with a high potential barrier, the paint comprises restacked sheets that force a percolating current through the layer and through the polymer connections between grains, wherever it exists. Estimates of conductivity variation with the length of the nanosheet paint in Fig. 5(c) follow a linear reduction (~3-fold decrease in conductivity with ~3-fold increase in distance). Paints deposited with various lengths so that the aspect ratio is controlled also exhibit the highest conductivity at aspects ratios close between 1-2×. In such cases, the direction of the applied paint preferentially orients the nanosheet stacks for increased conductance in one direction; longer painted strips increase the overall net resistance. At low aspect ratios, more percolating pathways exists over the length of the strip to provide minimum resistance.

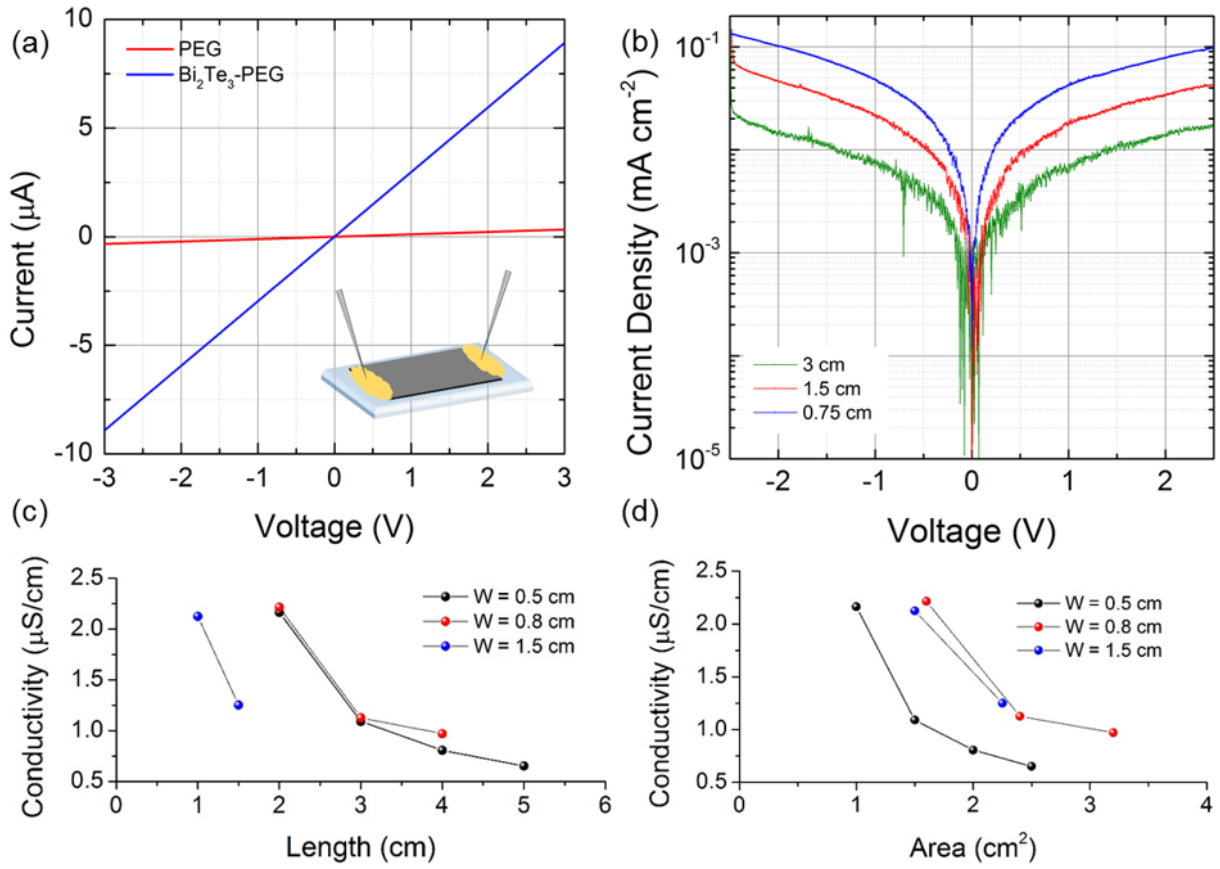

Figure 5 (a) I-V measurements showing the conductivity of the PEG400 vs a Bi_2Te_3-PEG composite. (b) J-V plot showing the change in conductivity with different lengths and also the existence of a non-zero current when crossing V=0. Conductivity variation as a function of (c) length and (d) area for nanosheet paints.

In dc I-V measurements acquired with a constant potential sweep rate, we consistently observe an ohmic response. As shown in Fig. 5(b), in some cases a positive current is found when crossing V = 0, which is understood to be linked to ionic or electronic traps that lags the applied voltage. Specific details on this phenomenon will be presented elsewhere, but it is characteristic of the PEG-Bi_2Te_2 2D system where the PEG is not intercalatively involved in any host-guest charge transfer interactions that fundamentally alter the conductivity of the Bi_2Te_3 nanosheets.

For Bi_2Te_3-PEG, mechanisms that contribute to electronic and ionic transport in these compounds needs to be considered. In a restacked layered assembly via mixing with a non-conducting polymer, the electronic transport is efficient along the layers but limited in the perpendicular direction. (47) Grain boundaries also form inter-grain contacts, increasing the overall resistivity as a function of length (determined to be quasi-linear for a given thickness in this system). Ionic transport plays a minimal role and generally limited to regions between sheets, which end unless the next nearest neighbouring sheets all have interlayer gaps aligned to maintain ionic mobility. While polymer located between the grains of restacked and few-layer nanosheets aggregates, it facilitates inter grain contacts to maintain end-to-end conductivity though the painted

film. Effects of ionic conductivity are found in dc measurements of PEG-containing Bi_2Te_3 where there is no charge compensation, rather pegylation or coating around percolating nanosheet pathways. A rough expectation on the resulting effective electronic conductivity is several orders of magnitude higher than the gross dc conductivity of the compound, since the dc resistance is dominated by the inter-grain resistance (the transient ionic conductivity during bias switches are negligible).

Conclusions

This work proposes a facile method of fabrication of a thin conductive film of Bi_2Te_3 in a PEG encapsulate using an uncomplicated and easily reproducible painting method. We successfully created a method of solvent exfoliation of Bi_2Te_3 into solution-dispersible 2D nanosheets that can form a practical thin film that can be distributed across a surface. The films produced consisted of Bi_2Te_3 nanosheets encapsulated within a PEG 400 coating, which was spread across substrates to give conductive films. Due to its innovative deposition method the paint can be spread on a wide range of morphologies, even flexible substrates. The possibility of adding alternative polymers and conductive additives, and the possibility of using flexible substrates are presently being explored, to form a more stable and conductive thermoelectric material coating for use in heat producing devices for energy harvesting and storage applications.

Acknowledgements

We acknowledges the support of the Irish Research Council Enterprise Partnership Scheme with Analog Devices under award EPSPG/2011/160. Support from the UCC Strategic Research Fund, and from the Irish Research Council New Foundations Award are also acknowledged. This work was also supported by SFI under the National Access Programme (NAP 417).

References

1. I. Chowdhury, R. Prasher, K. Lofgreen, G. Chrysler, S. Narasimhan, R. Mahajan, D. Koester, R. Alley and R. Venkatasubramanian, *Nat. Nanotechnol.*, **4**, 235 (2009).
2. A. Majumdar, *Nat. Nanotechnol.*, **4**, 214 (2009).
3. A. Majumdar, *Science*, **303**, 777 (2004).
4. R. Venkatasubramanian, E. Siivola, T. Colpitts and B. O'Quinn, *Nature*, **413**, 597 (2001).
5. T. C. Harman, P. J. Taylor, M. P. Walsh and B. E. LaForge, *Science*, **297**, 2229 (2002).
6. B. Poudel, Q. Hao, Y. Ma, Y. Lan, A. Minnich, B. Yu, X. Yan, D. Wang, A. Muto, D. Vashaee, X. Chen, J. Liu, M. S. Dresselhaus, G. Chen and Z. Ren, *Science*, **320**, 634 (2008).
7. J. N. Coleman, M. Lotya, A. O'Neill, S. D. Bergin, P. J. King, U. Khan, K. Young, A. Gaucher, S. De, R. J. Smith, I. V. Shvets, S. K. Arora, G. Stanton, H.-Y. Kim, K. Lee, G. T. Kim, G. S. Duesberg, T. Hallam, J. J. Boland, J. J. Wang, J. F. Donegan, J. C. Grunlan, G. Moriarty, A. Shmeliov, R. J. Nicholls, J. M. Perkins, E. M. Grieveson, K. Theuwissen, D. W. McComb, P. D. Nellist and V. Nicolosi, *Science*, **331**, 568 (2011).
8. V. Nicolosi, M. Chhowalla, M. G. Kanatzidis, M. S. Strano and J. N. Coleman, *Science*, **340** (2013).

9. K. M. F. Shahil, M. Z. Hossain, D. Teweldebrhan and A. A. Balandin, *Applied Physics Letters*, **96** (2010).
10. M. Saleemi, M. S. Toprak, S. Li, M. Johnsson and M. Muhammed, *Journal of Materials Chemistry*, **22**, 725 (2012).
11. S. K. Mishra, S. Satpathy and O. Jepsen, *Journal of Physics: Condensed Matter*, **9**, 461 (1997).
12. L. D. Hicks and M. S. Dresselhaus, *Physical Review B*, **47**, 12727 (1993).
13. M. F. O'Dwyer, T. E. Humphrey and H. Linke, *Nanotechnology*, **17**, S338 (2006).
14. T. Sarnet, T. Hatanpää, E. Puukilainen, M. Mattinen, M. Vehkamäki, K. Mizohata, M. Ritala and M. Leskelä, *The Journal of Physical Chemistry A* (2014).
15. A.-L. Hansen, T. Dankwort, M. Winkler, J. Ditto, D. C. Johnson, J. D. Koenig, K. Bartholomé, L. Kienle and W. Bensch, *Chemistry of Materials*, **26**, 6518 (2014).
16. K. Kato, Y. Hatasako, M. Uchino, Y. Nakata, Y. Suzuki, T. Hayakawa, C. Adachi and K. Miyazaki, *Advanced Materials Interfaces*, **1**, 1300015 (2014).
17. M. Takashiri, S. Tanaka and K. Miyazaki, *Journal of Elec Materi*, **43**, 1881 (2014).
18. A. K. Geim and K. S. Novoselov, *Nat Mater*, **6**, 183 (2007).
19. K. S. Novoselov, A. K. Geim, S. V. Morozov, D. Jiang, M. I. Katsnelson, I. V. Grigorieva, S. V. Dubonos and A. A. Firsov, *Nature*, **438**, 197 (2005).
20. K. S. Novoselov, A. K. Geim, S. V. Morozov, D. Jiang, Y. Zhang, S. V. Dubonos, I. V. Grigorieva and A. A. Firsov, *Science*, **306**, 666 (2004).
21. H. Zou, D. M. Rowe and G. Min, *Journal of Crystal Growth*, **222**, 82 (2001).
22. D.-H. Kim, E. Byon, G.-H. Lee and S. Cho, *Thin Solid Films*, **510**, 148 (2006).
23. S. Li, M. S. Toprak, H. M. A. Soliman, J. Zhou, M. Muhammed, D. Platzek and E. Müller, *Chemistry of Materials*, **18**, 3627 (2006).
24. Y. Hernandez, V. Nicolosi, M. Lotya, F. M. Blighe, Z. Sun, S. De, I. T. McGovern, B. Holland, M. Byrne, Y. K. Gun'Ko, J. J. Boland, P. Niraj, G. Duesberg, S. Krishnamurthy, R. Goodhue, J. Hutchison, V. Scardaci, A. C. Ferrari and J. N. Coleman, *Nat Nano*, **3**, 563 (2008).
25. M. Chhowalla, H. S. Shin, G. Eda, L.-J. Li, K. P. Loh and H. Zhang, *Nat Chem*, **5**, 263 (2013).
26. R. He, T.-F. Chung, C. Delaney, C. Keiser, L. A. Jauregui, P. M. Shand, C. C. Chancey, Y. Wang, J. Bao and Y. P. Chen, *Nano Letters*, **13**, 3594 (2013).
27. R. He, S. Sucharitakul, Z. Ye, C. Keiser, T. Kidd and X. A. Gao, *Nano Res.*, 1 (2014).
28. M. Thripuranthaka, R. V. Kashid, C. Sekhar Rout and D. J. Late, *Applied Physics Letters*, **104** (2014).
29. D. Teweldebrhan, V. Goyal, M. Rahman and A. A. Balandin, *eprint arXiv: 0912.0560* (2009).
30. G. Basile, C. Bernardin and S. Olla, *Physical Review Letters*, **96**, 204303 (2006).
31. C. Diaz, V. Lavayen and C. O'Dwyer, *J. Solid-State Chem.*, **183**, 1595 (2010).
32. W.-L. Song, M.-S. Cao, M.-M. Lu, S. Bi, C.-Y. Wang, J. Liu, J. Yuan and L.-Z. Fan, *Carbon*, **66**, 67 (2014).
33. A. Noël, J. Faucheu, M. Rieu, J.-P. Viricelle and E. Bourgeat-Lami, *Composites Science and Technology*, **95**, 82 (2014).
34. N. Heeder, A. Yussuf, I. Chakraborty, M. P. Godfrin, R. Hurt, A. Tripathi, A. Bose and A. Shukla, *Composites Science and Technology*, **100**, 70 (2014).
35. L. Yang, Z. Wang, Y. Ji, J. Wang and G. Xue, *Macromolecules*, **47**, 1749 (2014).
36. J. S. Lee and Y. S. Ko, *Catalysis Today*, **232**, 82 (2014).

37. C. Díaz, V. Lavayen and C. O'Dwyer, *Journal of Solid State Chemistry*, **183**, 1595 (2010).
38. G. Gannon, C. O'Dwyer, J. A. Larsson and D. Thompson, *The Journal of Physical Chemistry B*, **115**, 14518 (2011).
39. C. O'Dwyer, G. Gannon, D. McNulty, D. N. Buckley and D. Thompson, *Chemistry of Materials*, **24**, 3981 (2012).
40. C. G. Wu, D. C. DeGroot, H. O. Marcy, J. L. Schindler, C. R. Kannewurf, Y. J. Liu, W. Hirpo and M. G. Kanatzidis, *Chemistry of Materials*, **8**, 1992 (1996).
41. V. Petkov, V. Parvanov, P. Trikalitis, C. Malliakas, T. Vogt and M. G. Kanatzidis, *Journal of the American Chemical Society*, **127**, 8805 (2005).
42. S. Jiang, Z. Li, S. Huang, S. Lu, Y. Yu, G. Mou, J. Xu, Q. Zhu, X. Tan, X. Zhu and G. S. Zakharova, *Journal of The Electrochemical Society*, **161**, H684 (2014).
43. J. N. Coleman, S. Curran, A. B. Dalton, A. P. Davey, B. McCarthy, W. Blau and R. C. Barklie, *Physical Review B*, **58**, R7492 (1998).
44. S. De, P. J. King, P. E. Lyons, U. Khan and J. N. Coleman, *ACS Nano*, **4**, 7064 (2010).
45. S. De and J. N. Coleman, *ACS Nano*, **4**, 2713 (2010).
46. D. Stauffer, *Physica A: Statistical Mechanics and its Applications*, **210**, 317 (1994).
47. C. Glynn, D. Thompson, J. Paez, G. Collins, E. Benavente, V. Lavayen, N. Yutronic, J. D. Holmes, G. Gonzalez and C. O'Dwyer, *Journal of Materials Chemistry C*, **1**, 5675 (2013).